



# Modification and verification of the Deshpande–Fleck foam model: A variable ellipticity

Changfeng Zhu<sup>a</sup>, Zhijun Zheng<sup>a,\*</sup>, Shilong Wang<sup>b</sup>, Kai Zhao<sup>a</sup>, Jilin Yu<sup>a</sup>

<sup>a</sup> CAS Key Laboratory of Mechanical Behavior and Design of Materials, Department of Modern Mechanics, University of Science and Technology of China, Hefei 230026, China

<sup>b</sup> School of Civil Engineering, Anhui University of Technology, Maanshan 243032, China

## ARTICLE INFO

### Keywords:

Metal foam  
Constitutive model  
Deshpande–Fleck model  
Ellipticity  
Plastic Poisson's ratio  
Finite element simulation

## ABSTRACT

The ellipticity involved in the Deshpande–Fleck foam model describing the constitutive behaviour of cellular materials was usually considered to be constant, but some very different values were suggested in the literature. A cell-based finite element model of closed-cell foam under uni-/multi-axial compression is employed to verify the Deshpande–Fleck foam model. The ellipticity is determined by applying uniaxial and hydrostatic compression tests and it is found to vary with the equivalent plastic strain, i.e., the ellipticity decreases with the equivalent plastic strain and then increases sustainably before full densification. According to the understandings from the numerical results, a fitting relation between the ellipticity and the equivalent plastic strain is suggested. The ellipticities of an open-cell foam and a closed-cell foam studied experimentally in the literature are fitted well with this relation. A modification to the Deshpande–Fleck foam model with a variable ellipticity is thus proposed. The modified Deshpande–Fleck foam model brings much accurate predictions with using a rigid–plastic hardening (R-PH) idealisation model, which describes the stress–strain relation of cellular material under uniaxial compression. Good agreement is also observed between the experimentally measured stress–strain responses and the predictions of the modified Deshpande–Fleck foam model, especially when considering the effect of the plastic Poisson's ratio with a non-associated flow rule. The findings herein are helpful to improve the prediction accuracy of the Deshpande–Fleck foam model.

## 1. Introduction

Cellular materials (e.g., metal foam) have been widely used in industry for their lightweight and superior energy absorption capability [1, 2]. The stress–strain relation of cellular materials under uniaxial compression can be described by several phenomenological models, such as Rusch model [3, 4], Hanssen model [5], Liu model [6] and Avallé model [7]. Some stochastic constitutive models were developed to describe the mechanical responses of disordered cellular materials [8, 9]. However, these researches are focused mainly on the uniaxial compression behaviour of cellular materials. As cellular materials used in the engineering fields may be often subjected to complex loads, understanding the mechanical behaviours of cellular materials under multi-axial loading is beneficial to their engineering design.

Metal foams can yield under hydrostatic pressure due to their compressibility, which is very different from that of dense metals. So, the traditional theory of metal plasticity fails to extend to metal foams. The mean stress should be considered to understand the constitutive behaviour of metal foams. Many yield criteria and subsequent yield sur-

faces were developed to describe the stress state of cellular material under complex loads. Some suggested forms of the relation between the von Mises effective stress  $\sigma_e$  and the mean stress  $\sigma_m$  have been proposed to describe the yield surface of cellular materials [1, 2, 10–14]. Two kinds of commonly used yield functions are parabolic and elliptic.

A parabolic yield criterion was proposed by Gibson et al. [1, 2]

$$\sigma_e/\sigma_{pl} + 0.81\rho(\sigma_m/\sigma_{pl})^2 = 1, \quad (1)$$

where  $\sigma_{pl}$  is the magnitude of the uniaxial compression plateau stress and  $\rho$  the relative density of cellular material. This yield criterion is known as the GAZT model and it is only suitable for regular open-cell foams especially without imperfection [15, 16]. An improved parabolic yield function for metal foams was introduced by Miller [10] using the modified Drucker–Prager yield criterion. The yield function was written as

$$\sigma_e - b\sigma_m + \frac{c}{d}\sigma_m^2 - d = 0, \quad (2)$$

where  $b$ ,  $c$  and  $d$  are three material parameters. The initial yield surface of this model is in fact a translation of the GAZT yield surface on the

\* Corresponding author.

E-mail address: [zjzheng@ustc.edu.cn](mailto:zjzheng@ustc.edu.cn) (Z. Zheng).

axis of mean stress  $\sigma_m$ , and the subsequent yield surfaces are controlled by the equivalent plastic strain and the volumetric strain.

A self-similar isotropic hardening model was developed for metal foams by Deshpande and Fleck [11]. In this model, a popular elliptic yield surface was proposed, written as

$$\sqrt{\sigma_e^2 + \alpha^2 \sigma_m^2} - \sqrt{1 + (\alpha/3)^2} Y = 0, \quad (3)$$

where  $\alpha$  is the ellipticity of the ellipse representing the shape of the yield surface and  $Y$  the uniaxial yield stress of the material. This yield surface evolves in a geometrically self-similar manner which is governed by the equivalent plastic strain and it will be referred to as the Deshpande–Fleck foam model or D–F model in the remaining discussion. Deshpande and Fleck [11] also proposed a more complex differential hardening model, assuming hydrostatic yield strength and shear strength evolve independently. This differential hardening model has been rarely used although it can describe the yield process better, because it requires complex characteristic experiments to determine the parameters of the initial and subsequent yield surfaces.

Further considering the modified von Mises yield function of Drucker and Prager, Chen and Lu [12] introduced another elliptical yield function

$$\sigma_e^2 + (\gamma^2 + A(\hat{\epsilon}))\sigma_m^2 - B(\hat{\epsilon}) = 0, \quad (4)$$

where  $\hat{\epsilon}$  is the characteristic strain defined as  $\hat{\epsilon} = \sqrt{\epsilon_e^2 + \epsilon_v^2/\gamma^2}$ , with von Mises effective strain  $\epsilon_e$ , volumetric strain  $\epsilon_v$  and elastic material parameter  $\gamma$ . The evolution of the yield surface is governed by the characteristic strain, and the variable material parameters  $A$  and  $B$  are both related to the characteristic strain.

The Deshpande–Fleck foam model attracts a lot of attention because it can describe the response of metal foams under multi-axial loading approximately and it only has two parameters, i.e., the ellipticity  $\alpha$  and the uniaxial yield stress  $Y$ . In the literature, the ellipticity  $\alpha$  was considered as a constant in subsequent yield and the associated flow rule was assumed. Recently, the initial elliptical yield surface of this model has been verified by more and more experimental tests and numerical simulations [16–22]. The Deshpande–Fleck foam model has also been successfully applied to and widely used in some commercial finite element softwares, see the crushable foam model with isotropic hardening in ABAQUS and the Deshpande–Fleck foam model in LS-DYNA [23–26]. Two typical measurements were conducted to probe the yield surface using a high pressure triaxial system by Deshpande and Fleck [11], i.e., the specimen was pressurized to a level of axial strain and the pressure was then decreased slowly until zero and the other was started at the uniaxial compression and slowly built up the pressure.

The ellipticity involved in the Deshpande–Fleck foam model is not easy to determine. It was taken as a constant as the shapes of yield surfaces almost do not change with the axial strain for a primary loading path of uniaxial compression. Therefore, the ellipticity of the initial yield surface is often used to replace the ellipticity of the subsequent yield surface. However, the evolution of the yield surface in the Deshpande–Fleck foam model is governed by the equivalent plastic strain defined by the equivalent plastic work, which has contributions from both the deviatoric plastic strain and the volumetric plastic strain. In fact, the yield surface elongates along the axis of mean stress with the volumetric strain for a primary loading path of hydrostatic compression. So, it is doubtful whether the ellipticity does not vary with the equivalent plastic strain.

The ellipticity  $\alpha$  was considered to be dependent on the plastic Poisson’s ratio  $\nu^p$  with an associated flow rule [11, 26], written as

$$\alpha^2 = \frac{9(1 - 2\nu^p)}{2(1 + \nu^p)}. \quad (5)$$

This formula has been widely used. However, the plastic Poisson’s ratio, defined as the negative value of the ratio of the transverse and axial logarithmic strain rates, is hard to measure and the experimental

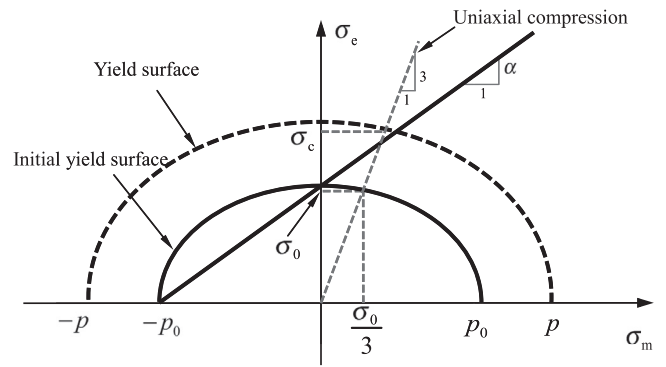


Fig. 1. Yield surfaces for the Deshpande–Fleck foam model.

results were scattered. So, significantly different values of the ellipticity  $\alpha$  were suggested in the literature [11, 17, 20, 26], even for identical metal foams produced by the same company. The associated flow “proved” by the consistency of independently measured values of the plastic Poisson’s ratio and the ellipticity is questionable [11]. Another formula was introduced by Vural and his co-workers [27–29], i.e.,

$$\alpha^2 = \frac{9(1 - 2\nu)}{2(1 + \nu)}, \quad (6)$$

where  $\nu$  is the elastic Poisson’s ratio of foam. It is questionable to use elastic parameters to characterize the plastic stage, although sometimes this formula has a better approximation.

Another way to determine the shape parameter ellipticity is based on two chosen points on the ellipse [11, 19], written as

$$\alpha^2 = \frac{9\sigma_0^2}{9p_0^2 - \sigma_0^2}, \quad (7)$$

where  $\sigma_0$  and  $p_0$  are the initial yield stress in uniaxial compression and in hydrostatic compression, respectively. This method is adopted in ABAQUS [23]. However, the stress–strain curves of many foam samples do not show a clear yield point, and the value of initial yield stress cannot be determined accurately in many practical cases. More importantly, all of the methods mentioned above assume that the ellipticity remains constant in successive yielding. In fact, the ellipticity  $\alpha$  is obviously related to the material’s compressibility and the compressibility varies with the plastic strain [26]. So, the ellipticity may be a variable value associated with the plastic strain.

In this study, the ellipticity involved in the Deshpande–Fleck foam model is determined by virtual uni-/multi-axial compression tests using cell-based finite element models. A modified Deshpande–Fleck foam model is proposed by considering a variable ellipticity. A much accurate material model is employed to describe the stress–strain relation of cellular material under uniaxial compression. The modified Deshpande–Fleck foam model is verified by cell-based finite element models. Some experimental data in the literature are taken for comparison to verify the modified Deshpande–Fleck foam model with a non-associated flow rule.

## 2. Constitutive models

### 2.1. The Deshpande–Fleck foam model

The Deshpande–Fleck foam model assumes similar behaviours in compression and tension, as depicted in Fig. 1. The D–F model is an elliptic yield surface in the von Mises effective stress vs. mean stress plane and assumes the ellipticity remains constant. In this study, compression is taken as positive. The elliptic yield surface is centered at the origin in the  $\sigma_e$ – $\sigma_m$  stress plane and evolves in a self-similar manner governed by the equivalent plastic strain. After comparing with other independent variables, Deshpande and Fleck noted that the scheme of

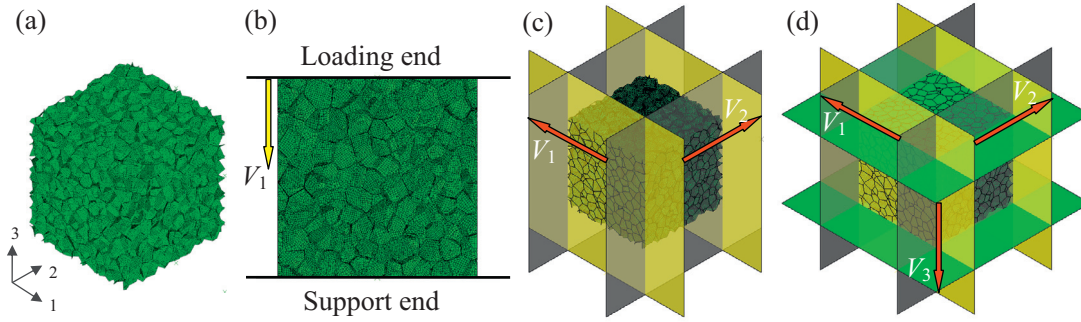


Fig. 2. A cell-based finite element model of (a) Voronoi foam, (b) uniaxial compression, (c) biaxial compression and (d) triaxial compression.

using the equivalent plastic strain was found to give better agreement with the available experimental data, see the note in page 1272 of Ref. [11]. The equivalent plastic strain rate  $\dot{\epsilon}^p$  is defined according to the equivalent plastic work rate, i.e.,  $\sigma_c \dot{\epsilon}^p = \sigma_{ij} \dot{\epsilon}_{ij}^p$ , where  $\sigma_c$  is the uniaxial compression stress associated to current yield surface,  $\sigma_{ij}$  and  $\dot{\epsilon}_{ij}^p$  are tensors of stress and plastic strain rate respectively with  $i, j = 1, 2, 3$ . The elastic strain is assumed to be negligibly small in the present model, so that the total strain equals the plastic strain. In the following discussion,  $\bar{\epsilon}$  is adopted to represent the equivalent plastic strain.

The elliptical yield function of the D–F model is defined as

$$\sqrt{\sigma_e^2 + \alpha^2 \sigma_m^2} - F = 0, \tag{8}$$

where  $F$  is the semi axis length of the yield ellipse on the  $\sigma_e$ -axis and the shape parameter, i.e., ellipticity  $\alpha$ , is defined as the aspect ratio of the yield ellipse. The mean stress and the von Mises effective stress in uniaxial compression are  $\{\sigma_m, \sigma_e\} = \{\sigma_c/3, \sigma_c\}$ . Thus, the yield surface can be re-written as Eq. (3). For the low-density metal foams used in the following numerical simulations,  $\sigma_0$  almost equals to  $p_0$ , and thus leads to  $\alpha^2 \approx 9/8$ . However, when the plastic Poisson's ratio is nearly zero,  $\alpha^2$  is  $9/2$  according to Eq. (5), which illustrates Eq. (5) deduced from an associated flow rule may be invalid. For this geometrically self-similar model, two loading scenarios are sufficient to determine all parameters. Deshpande and Fleck [11] also proposed a more sophisticated differential hardening model whose yield surface elongates at different rates along the hydrostatic and deviatoric axes. The evolution of this yield surface is governed by two parameters, which needs at least three different loading scenarios to determine all parameters and the determination of parameters requires iterative process. This differential hardening model has been rarely used due to its complexity. The present study only revisits the self-similar model mentioned above.

### 2.2. Predictions of typical loadings

The mean stress and the von Mises effective stress under a specific loading condition can be expressed by  $\sigma_c$  according to the D–F model, provided the direction of multi-axial loading is known. The stress triaxiality,  $\eta = \sigma_m / \sigma_e$  [11], is widely used to characterize the direction of loading, ranging from  $\eta = 1/3$  for uniaxial compression to  $\eta \rightarrow \infty$  for hydrostatic compression. From the D–F model with a specific value of  $\eta$ , the von Mises effective stress and the mean stress can be calculated as

$$\begin{cases} \sigma_e = \sigma_c \sqrt{\frac{1+\alpha^2/9}{1+\eta^2\alpha^2}} \\ \sigma_m = \eta \sigma_c \sqrt{\frac{1+\alpha^2/9}{1+\eta^2\alpha^2}} \end{cases} \tag{9}$$

It can be seen clearly that the uniaxial compression stress on the yield surface is essential for the calculation of the mean stress and the von Mises effective stress. Under hydrostatic compression, i.e.,  $\eta \rightarrow \infty$ ,

one has  $\sigma_e = 0$  and

$$\sigma_m = p = \sigma_c \sqrt{\frac{1}{\alpha^2} + \frac{1}{9}}, \tag{10}$$

where  $p$  is the value of hydrostatic pressure.

### 2.3. Uniaxial compression stress–strain relation

Metal foams can absorb massive energy with large plastic deformation and in this process the elastic deformation may be ignored. For simplicity, metal foams are usually modelled as a rigid–plastic hardening (R-PH) idealisation. Recently, Zheng et al. [30] proposed a very simple R-PH model to describe the uniaxial compression behaviour of cellular materials, in which the nominal stress–strain relation is expressed as

$$\sigma_n = \sigma_{n0} + \frac{C \epsilon_n}{(1 - \epsilon_n)^2}, \tag{11}$$

where subscript  $n$  denotes nominal,  $\sigma_{n0}$  is the nominal initial crushing stress and  $C$  the strain hardening parameter. The elastic strain is assumed to be negligibly small in the present model so that the axial total strain equals the axial plastic strain. It is easy to see that the equivalent plastic strain is equal to the axial plastic strain in uniaxial compression. So, in this case, we have  $\epsilon = \epsilon^p = \bar{\epsilon}$ . The relation between the true (logarithmic) plastic axial strain  $\epsilon$  and the nominal strain can be expressed as  $\epsilon = -\ln(1 - \epsilon_n)$ . Then, the true stress–true strain relation can be expressed as

$$\sigma_c = \frac{\sigma_{n0} + C(e^{2\epsilon} - e^\epsilon)}{[1 + \nu^p - \nu^p \exp(-\epsilon)]^2}. \tag{12}$$

It is considered that the true stress almost equals the nominal stress since there is no significant expansion of the cross section during the compression process of low-density foams [10, 16, 30–33]. So, the R-PH model can also be re-written approximately as  $\sigma_c = \sigma_{n0} + C(e^{2\epsilon} - e^\epsilon)$ . There are only two material parameters in Eq. (11) and their values will be determined by applying cell-based finite element method as follows.

## 3. Numerical methods

### 3.1. Cell-based finite element model

The 3D Voronoi technique was applied to generate random foams in simulations, as done in Ref. [30]. Three random samples of Voronoi structures were used in this study to measure the scatter of samples. Numerical simulations of closed-cell foam under uni-/multi-axial compression were implemented with finite element code ABAQUS/Explicit. In this study, the specimen is a  $30 \times 30 \times 30 \text{ mm}^3$  cube with 1200 nuclei and the irregularity is 0.4, see Fig. 2(a). The cell-wall thickness of the specimen is uniform and is dependent on the relative density  $\rho$  of the specimen, e.g., the relative density of the specimen is set as 0.1

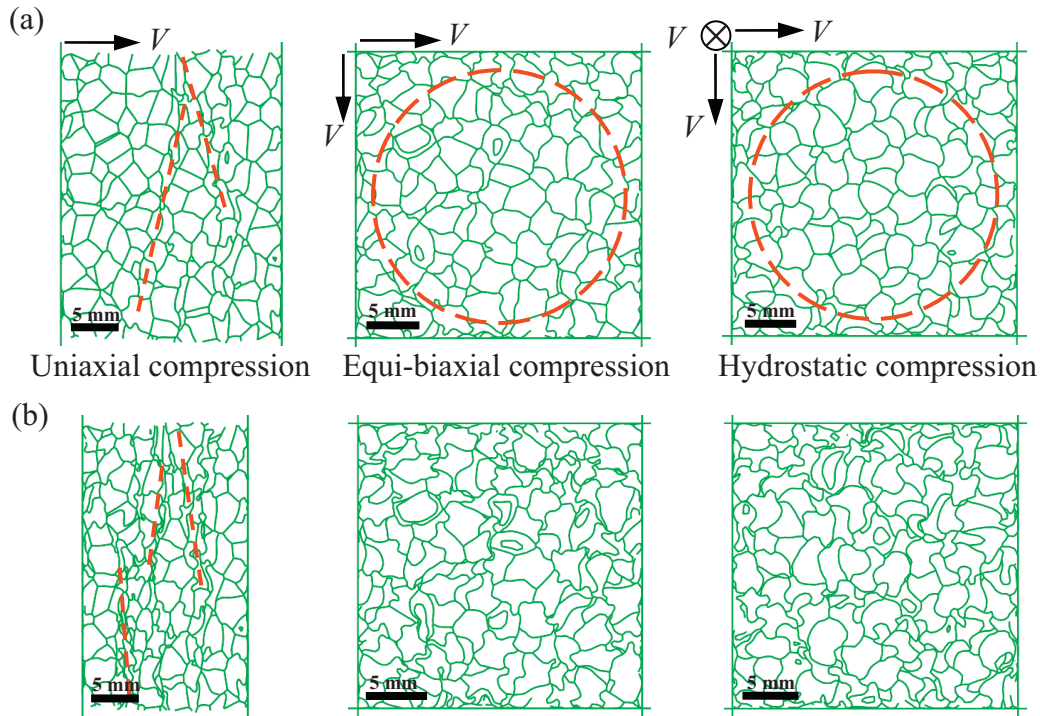


Fig. 3. Cross-sectional deformable patterns of foam specimens under three typical compressive loads when nominal volumetric strain is (a)  $\epsilon_{nv} = 0.2$  and (b)  $\epsilon_{nv} = 0.4$ .

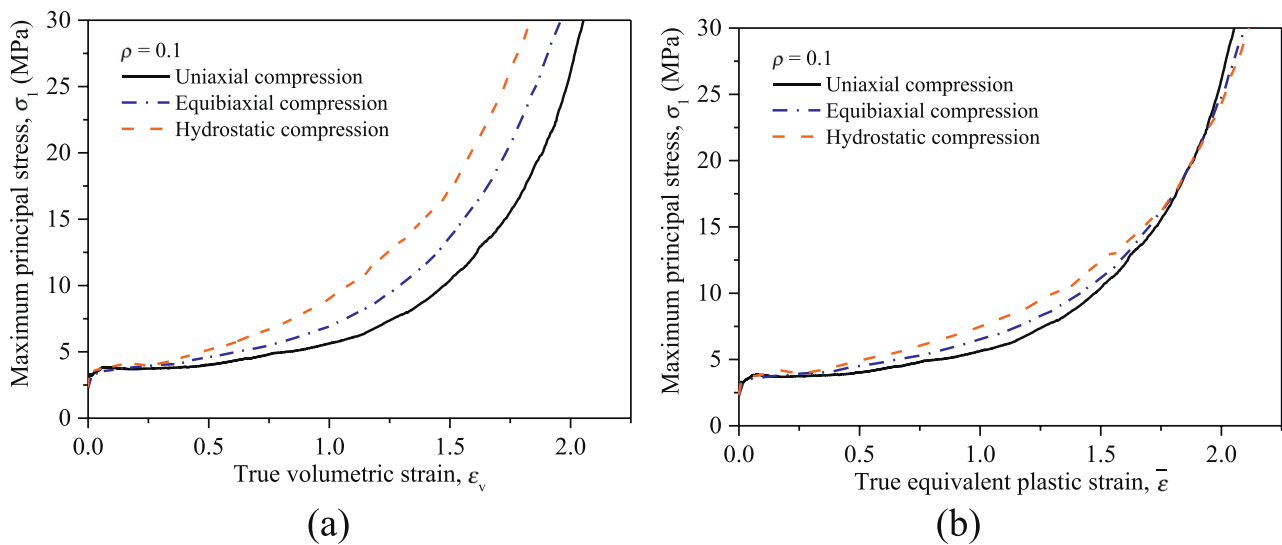


Fig. 4. Variations of the maximum principal stress of foam specimens under three typical compressive loads with (a) the true volumetric strain and (b) the true equivalent plastic strain.

and cell-wall thickness is about 0.0993 mm. Different relative densities of specimens with similar mesostructures can be obtained by changing the cell-wall thickness of a generated Voronoi structure. The cell walls are meshed with hybrid shell elements of types S4R and S3R and the characteristic size of shell elements is set to be about 0.3 mm through a mesh sensitivity study [30]. Shell elements with sharp angles are eliminated for saving computer time and finally the specimens used has about 274,000 shell elements, including about 60,000 S3R elements and 214,000 S4R elements. The matrix material aluminium is taken to be rate-independent, elastic-linear plastic hardening and the material parameters of density  $\rho_s = 2700 \text{ kg/m}^3$ , Young's modulus  $E = 70 \text{ GPa}$ , Poisson's ratio  $\nu = 0.33$ , yield stress  $\sigma_{ys} = 80 \text{ MPa}$  and Tangent modulus  $E_{tan} = 30 \text{ MPa}$  respectively, in which the virtual uniaxial compression ex-

perimental data of the 3D Voronoi foam agreed well with the uniaxial compression experimental data [15].

A pair of rigid plates is employed on the top and bottom of a foam specimen to apply quasi-static uniaxial compression, as shown in Fig. 2(b). A rigid plate is fixed, while the other one moves with a constant velocity of 10 m/s, perpendicular to the fixed rigid plate. Two pairs of rigid plates are employed to apply biaxial compression, as depicted in Fig. 2(c). Similarly, three pairs of rigid plates are used for triaxial loading, as shown in Fig. 2(d). In one direction of every pair of rigid plates, one plate is fixed, while the other moves with a constant velocity. The speed of moving rigid plate is no more than 10 m/s, which ensures the stress balance between the support end and the loading end of each direction during the whole loading process. General contacts were applied

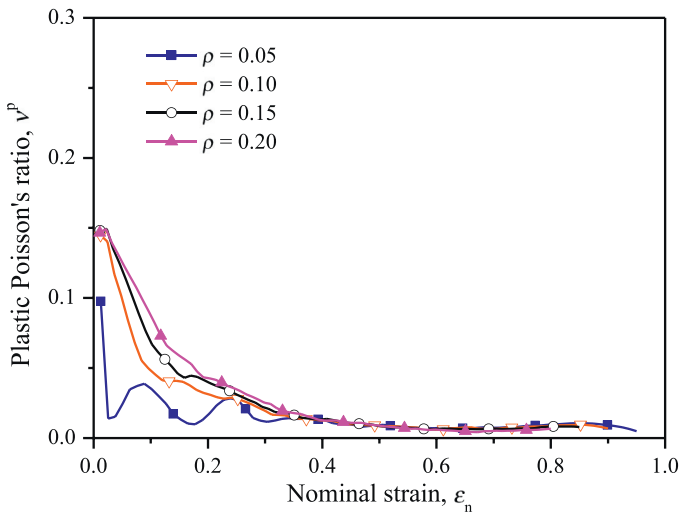


Fig. 5. Variations of the plastic Poisson's ratios with the nominal strain for foam specimens having different relative densities.

to all possible contact, with a friction coefficient of 0.2 between shell elements and without friction between rigid plates and the foam. Displacement controlled loading is applied in numerical simulations. This controlled loading method is also recommended to experimental tests, although it is hard to realize, as the stress controlled loading may cause inhomogeneous overall deformation, e.g., see Fig. 13 in Ref. [5].

3.2. Deformation patterns under uniaxial, equi-biaxial and hydrostatic compression

Uniaxial, equi-biaxial and hydrostatic compressions of a foam specimen with a relative density of 0.1 are selected as three typical loading scenarios here. The speed of moving rigid plates is 10 m/s and the image of an identical middle section is used to represent deformation characteristics. Different deformation patterns are observed under uniaxial, biaxial and triaxial compressions, as shown in Fig. 3. At the very beginning of the three loading scenarios, the deformation all starts from the place close to the rigid plates, which is because the cut cells are weaker than the complete ones. With the continuation of compression, e.g. when nominal volumetric strain  $\epsilon_{nv} = 0.2$ , it can be seen from Fig. 3(a) that

the deformation consists of randomly distributed shear collapse bands in uniaxial compression, as reported in Ref. [30]. Under multi-axial compression, however, the shear collapse bands are concentrated near the rigid plates and they form a circular feature in deformation. The intersecting of shear collapse bands may strength the foam specimen to block further local deformation. When the macroscopic deformation increases, more shear collapse bands are observed under uniaxial compression while the circular shear band disappears under equi-biaxial and hydrostatic compressions. The existence of rigid plates hinders the free development of shear collapse bands and makes the whole specimen in a more uniform deformation state, as shown in Fig. 3(b). Shear collapse bands are induced by the deformation of surrounding relatively weak cells due to minimal energy consumption, and the maximum principal stress is dependent on the strength of the weakest links. Another obvious difference between multi-axial and uniaxial compressions is that almost all the cell walls are bent under multi-axial compression, but only the cell walls near the shear bands are bent under uniaxial compression. It indicates that the deformation under multi-axial compression tends to be much homogeneous. Under uniform deformation, the ability to resist deformation of relatively weak cells is averaged by the strong cells, so the whole specimen shows a higher ability to resist deformation. The more rigid plates there are, the more uniform the deformation of the specimen. That may be the deformation mechanisms to the maximum principal stress of hydrostatic compression larger than the equi-biaxial compression which is larger than the uniaxial compression when taking the true volumetric strain as an independent variable, as shown in Fig. 4(a). As a comparison, the maximum principal stress by taking the true equivalent plastic strain as an independent variable is shown in Fig. 4(b).

Uniaxial compression Equi-biaxial compression Hydrostatic compression

The plastic Poisson's ratio of foam specimens under uniaxial compression, which is defined as the negative ratio of the transverse logarithmic strain rate to the axial logarithmic strain rate [11], is found to be very small, as illustrated in Fig. 5. So, the plastic Poisson's ratio is assumed to be zero in the analysis of the numerical simulations.

3.3. Fitting parameters for the R-PH model

The nominal stress–strain data of the foam specimens with different relative densities under virtual uniaxial compression were used to fit the R-PH model. It is found that the R-PH model can fit the quasi-static nominal stress–strain relation very well, as shown in Fig. 6(a). It

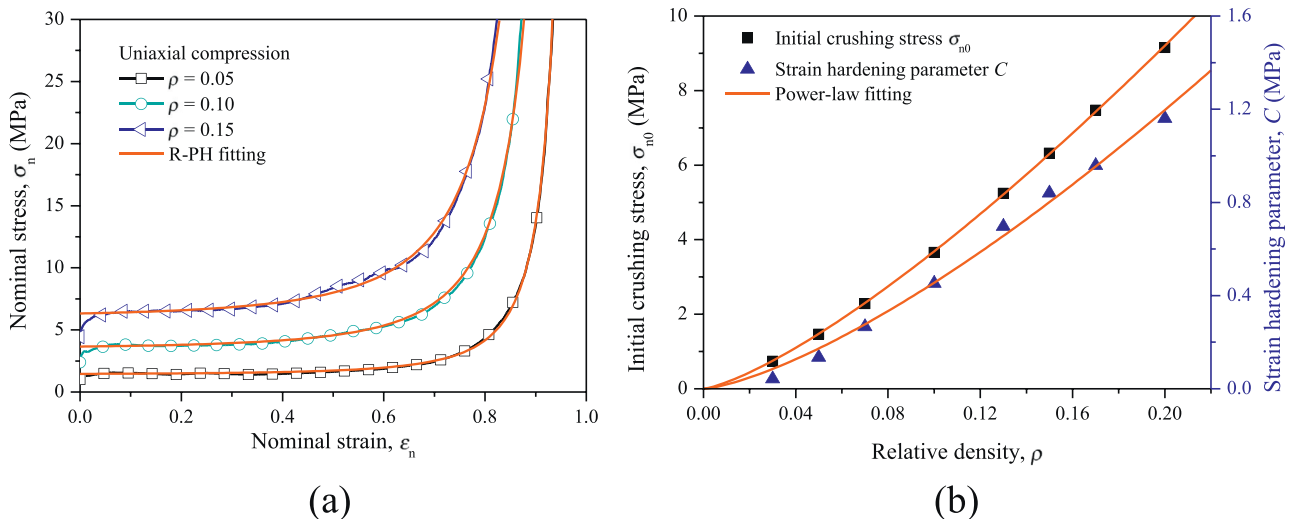


Fig. 6. (a) Nominal stress–strain relations for the Voronoi models with different relative densities under uniaxial compression and (b) fitting parameters of the R-PH model.

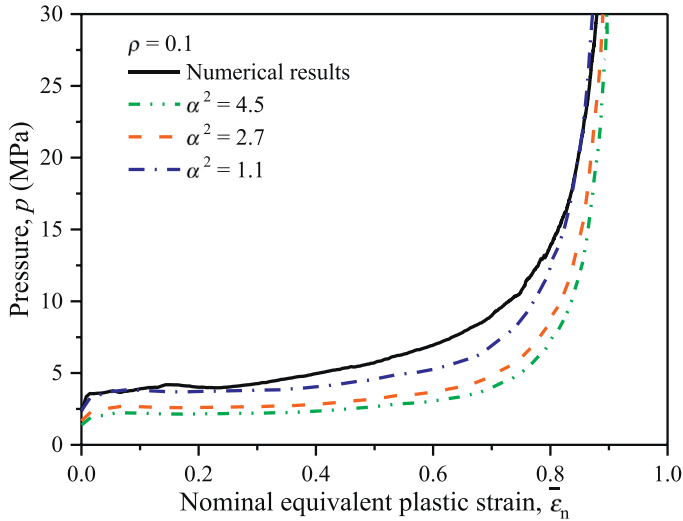


Fig. 7. Predictions of hydrostatic pressure using different values of the ellipticity  $\alpha$ .

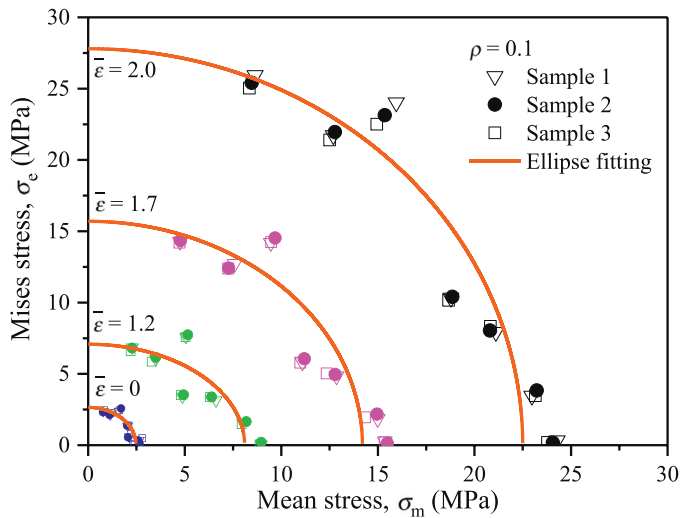
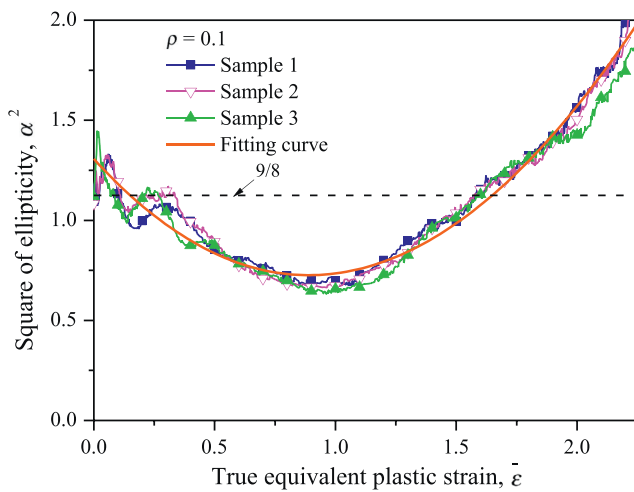
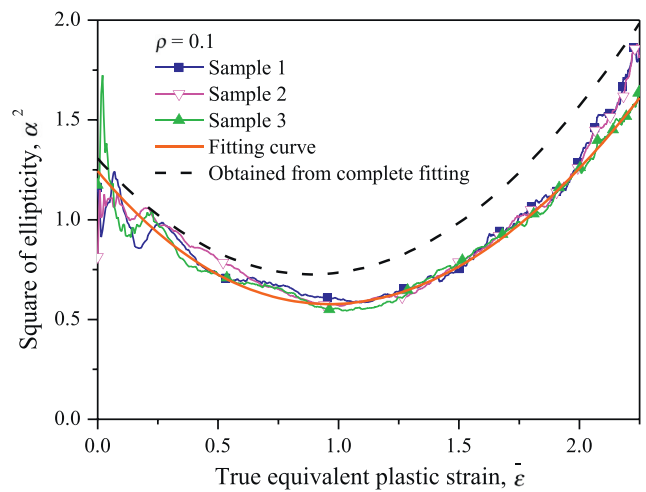


Fig. 8. A schematic diagram of ellipse fitting for three different samples with the equivalent plastic strains of 0, 1.2, 1.7 and 2.0.



(a)



(b)

Fig. 9. Fitting of  $\alpha^2$  determined by (a) complete fitting and (b) Eq. (16).

should be noted that in the fitting process the two material parameters are determined as follows. The initial crush stress  $\sigma_{n0}$  is obtained by the average of stress in a small plastic strain range of the initial crushing stage, here up to a nominal plastic strain of 0.2 is considered. The strain hardening parameter  $C$  is determined by applying the least squares fitting technique.

The two material parameters of the R-PH model,  $\sigma_{n0}$  and  $C$ , were found both related to the relative density of cellular material and can be expressed in the form of a power exponent [34], written as

$$\begin{cases} \sigma_{n0}(\rho) = \sigma_{ys} \cdot k_1 \rho^{n_1} \\ C(\rho) = \sigma_{ys} \cdot k_2 \rho^{n_2} \end{cases} \quad (13)$$

where  $\sigma_{ys}$  is the yield stress of matrix material,  $k_1$ ,  $k_2$ ,  $n_1$  and  $n_2$  are material parameters. By fitting the initial crushing stress and the strain hardening parameter of different relative densities in Fig. 6(b) with Eq. (13), we obtain  $k_1 = 0.963$ ,  $n_1 = 1.32$ ,  $k_2 = 0.141$  and  $n_2 = 1.39$ .

#### 4. Results and discussion

##### 4.1. A typical example with constant values of the ellipticity

Under hydrostatic compression, i.e., when  $\eta \rightarrow \infty$ , the mean stress is the value of hydrostatic pressure which can be deduced from Eq. (10) using the known uniaxial stress–strain relation. Different values of the ellipticity  $\alpha$ , i.e.,  $\alpha^2 = 4.5, 2.7$  and  $1.1$ , are obtained from Eqs. (5)–(7) with using the plastic Poisson’s ratio  $\nu^p = 0$ , the Poisson’s ratio  $\nu = 0.15$  and the relation of  $\sigma_0 = p_0$ , respectively. Predictions using these values of the ellipticity  $\alpha$  for a foam specimen with a relative density of 0.1 are illustrated in Fig. 7. It transpires that all the results do not provide any satisfactory prediction. This suggests a variable value of the ellipticity with the equivalent plastic strain, as discussed later.

##### 4.2. A modified relation of the ellipticity

A more accurate ellipticity  $\alpha$  can be calculated by fitting the yield ellipse. The mean stress and the von Mises effective stress obtained from different loading scenarios in the cell-based finite element simulations are fitted to the ellipse standard equation, and then the ellipticity  $\alpha$  is determined. Seven different loading scenarios are concerned, including two cases of proportional loading, i.e., uniaxial compression with

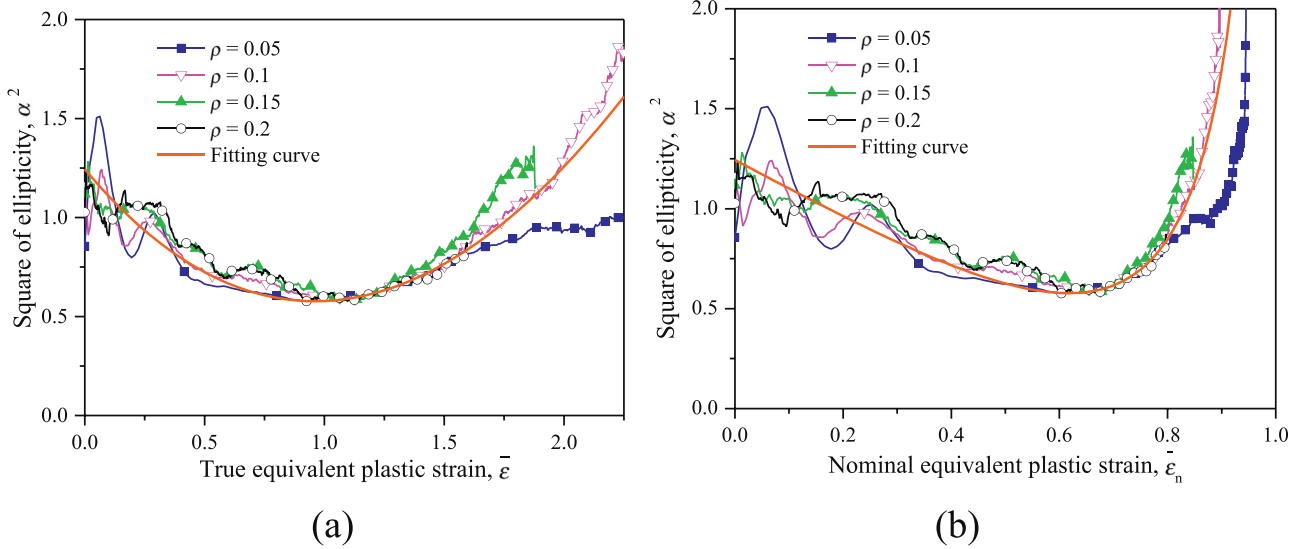


Fig. 10. Variations of the square of ellipticity  $\alpha^2$  for Sample 1 having different relative densities with (a) the true equivalent plastic strain and (b) the nominal equivalent plastic strain.

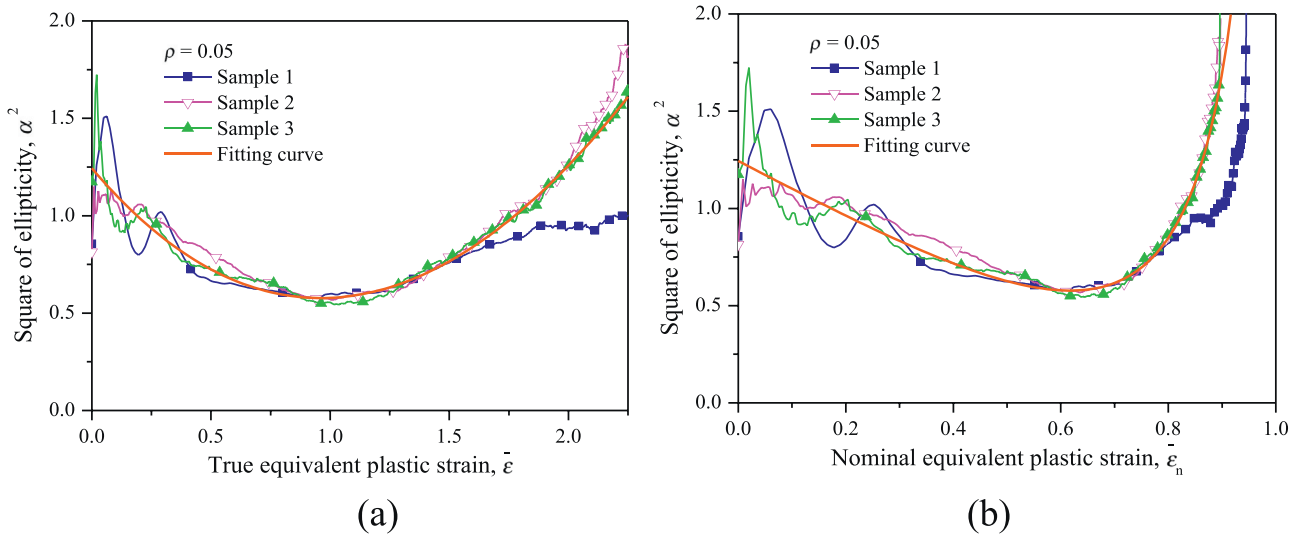


Fig. 11. Variations of the square of ellipticity  $\alpha^2$  for three different samples having a relative density of 0.05 with (a) the true equivalent plastic strain and (b) the nominal equivalent plastic strain.

$\eta = 1/3$  and hydrostatic compression with  $\eta \rightarrow \infty$ , and five cases of non-proportional loadings in which  $\eta$  is not constant, and the ratios of the velocities in the three principal stress directions are -0:5, -2:5, 0:0:5, 0:1:5 and 1:3:5, where “-” represents a free end (without constraint) and 0 is a fixed constraint end. For example, -0:5 and 0:0:5 are two kinds of passive multi-axial tests, i.e., one-side-displacement constrained and lateral-displacement constrained compression which are easy to implement [35]. Three different samples are employed to consider the scatter of samples.

As shown in Fig. 8, the mean stress and the von Mises effective stress of different loading scenarios are fitted by the ellipse standard equation at different true equivalent plastic strains of 0, 1.2, 1.7 and 2.

The variation of  $\alpha^2$  with the true equivalent plastic strain is independent of random sampling and the results show that  $\alpha^2$  is obviously not a constant, as depicted in Fig. 9(a). The square of ellipticity,  $\alpha^2$ , obtained from elliptic equation fitting, is originally close to 9/8, which means the deformation of three orthogonal directions indeed does not affect

each other at the very beginning, i.e., the plastic Poisson’s ratio is equal to zero approximately. It decreases with the increase of the equivalent plastic strain and then increases sustainably before full densification. According to the variation characteristics of  $\alpha^2$ , it is assumed that the fitting equation consists of three terms: an exponential term (decreasing), a quadratic term (increasing) and a constant term, i.e.,

$$\alpha^2 = b_1 e^{-b_2 \bar{\epsilon}} + b_3 \bar{\epsilon}^2 + b_4. \tag{14}$$

Fitting Eq. (14) with the data averaging of the three samples in Fig. 9(a), we obtain  $b_1 = 3.342$ ,  $b_2 = 0.3977$ ,  $b_3 = 0.5242$  and  $b_4 = -2.035$ .

According to the definition of isotropic ellipse yield surface, the ellipticity can also be determined by any two asymmetrical points of the ellipse, i.e.,  $\alpha^2$  can be determined by any two loading cases  $\{\sigma_{m1}, \sigma_{e1}\}$  and  $\{\sigma_{m2}, \sigma_{e2}\}$  associated with the same true equivalent plastic strain in the absence of a large amount of experimental data, written as

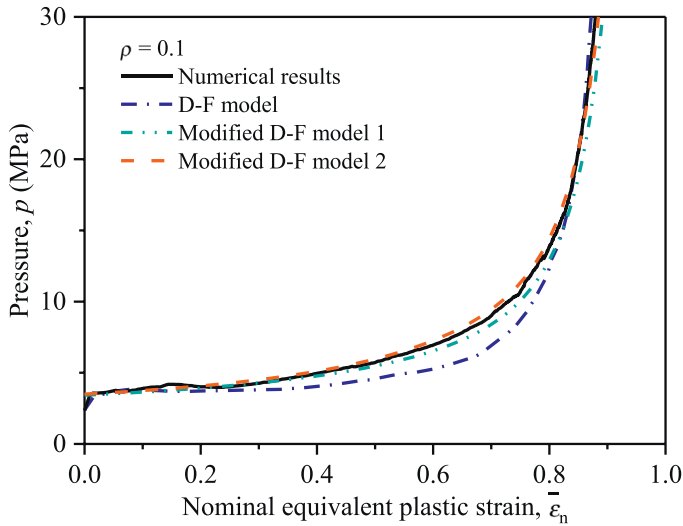


Fig. 12. Predictions of pressure under hydrostatic compression according to the D-F model and modified D-F model.

$$\alpha^2 = \frac{\sigma_{e2}^2 - \sigma_{e1}^2}{\sigma_{m1}^2 - \sigma_{m2}^2} \quad (15)$$

In particular,  $\alpha^2$  can be calculated according to

$$\alpha^2 = \frac{9\sigma_c^2}{9p^2 - \sigma_c^2} \quad (16)$$

when applying loading scenarios of uniaxial compression  $\{\sigma_{m1}, \sigma_{e1}\} = \{\sigma_c/3, \sigma_c\}$  and hydrostatic compression  $\{\sigma_{m2}, \sigma_{e2}\} = \{p, 0\}$ . This is the simplest way to determine  $\alpha^2$  experimentally. Compared to any other two loading scenarios, the value of  $\alpha^2$  calculated using Eq. (16) has a smaller error, since the two points of uniaxial compression and hydrostatic compression have the farthest distance in the von Mises effective stress vs. mean stress plane. In fact, Eq. (7), which has been used widely to calculate  $\alpha^2$ , is the special case of Eq. (16) when using the initial yield stresses in uniaxial and hydrostatic compressions. The calculated values of  $\alpha^2$  from Eq. (16) (based only on data from uniaxial and hydrostatic compressions, hereafter refers as two-point fitting) and the results from ellipse fitting (based on all data from different loading conditions,

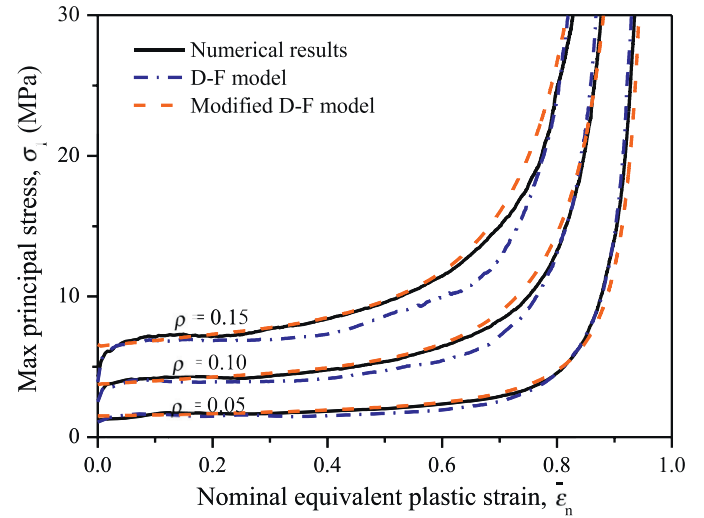
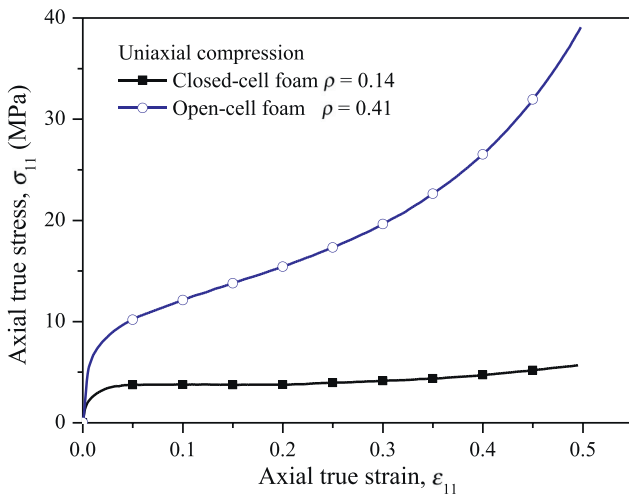


Fig. 13. Predictions of the maximum principal stress by the D-F model and the modified D-F model when the velocity ratio of three principal stress directions is 5:5:0.

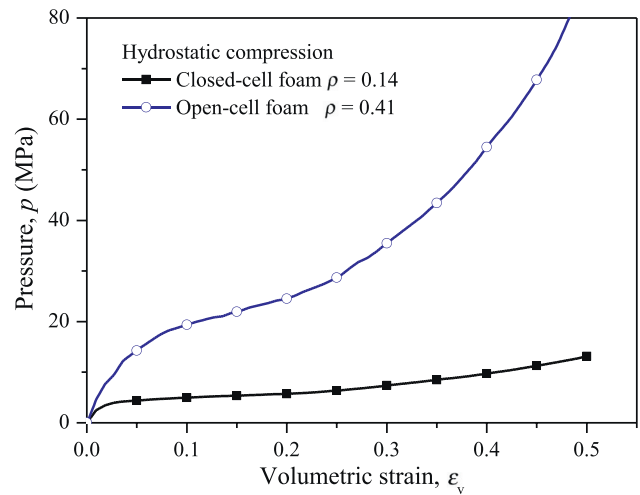
hereafter refers as complete fitting) are shown in Fig. 9(b) and (a), respectively. A comparison shows that the two-point fitting is a good approximation of the complete fitting, as illustrated in Fig. 9(b). Fitting Eq. (14) with the data in Fig. 9(b) leads to

$$\alpha^2 = 2.496e^{-0.5790\bar{\epsilon}} + 0.4314\bar{\epsilon}^2 - 1.252. \quad (17)$$

The values of  $\alpha^2$  calculated from Eq. (16) with different relative densities are shown in Fig. 10 by taking the true equivalent plastic strain or the nominal equivalent plastic strain as an independent variable. It is found that the relative density has a negligible effect on  $\alpha^2$  for Sample 1. The ellipticity is almost constant when the true equivalent plastic strain is very large for Sample 1 with a relative density of 0.05. This is resulted from the scatter of samples, since other two selected samples fit with Eq. (17) well, as shown in Fig. 11. Although different samples may produce different results, the scope of strain with almost constant ellipticity is very small, as illustrated in Fig. 10(b) with taking the nominal equivalent plastic strain as an independent variable. Ignoring this unimportant small area, we can obtain a very simple but well approxi-



(a)



(b)

Fig. 14. Stress–strain relations of closed-cell and open-cell foams under (a) uniaxial compression and (b) hydrostatic compression. The experimental data are extracted from Ref. [36].

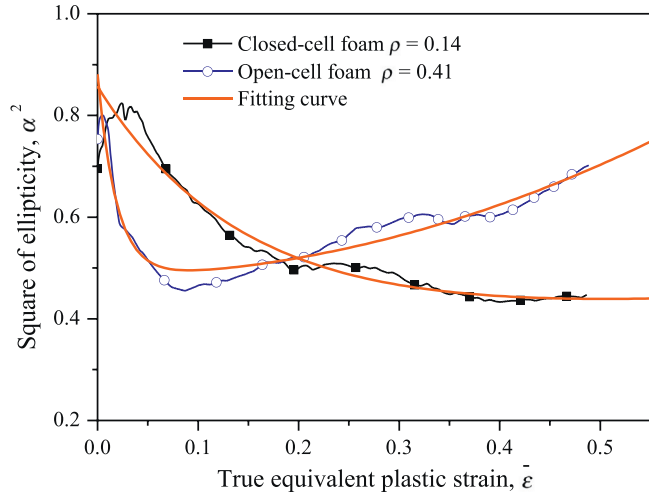


Fig. 15. Values of  $\alpha^2$  of two kinds of foams in Ref. [36].

mated equation. In the following, Eq. (17) will be used for the sake of simplification.

According to Eq. (10), the pressure under hydrostatic compression can be obtained with using the uniaxial stress and the ellipticity. In the D–F model, a constant  $\alpha^2 = 9/8$  and scattered data get from uniaxial compression of the cell-based finite element model are used. In the modified D–F model, we use the R-PH model to replace the uniaxial stress–strain relation of scattered points. Two curves of  $\alpha(\bar{\epsilon})$  are considered to replace a fixed value of  $\alpha$ . One is obtained by the complete fitting method and the other is by the two-point fitting method (Eq. (17)), which correspond to the modified D–F model 1 and 2 in Fig. 12 respectively. The nominal equivalent strain is obtained through coordinate transformation and details will be given in Section 4.3.

The pressure under hydrostatic compression predicted by the D–F model and the modified D–F model using the uniaxial compression stress–strain relation are compared with the virtual experiment in Fig. 12. The results show that the prediction of D–F model has a good agreement with the virtual experimental data when the strain is less than about 0.3, while the prediction is getting bad when the strain increases. The prediction is improved in the densification stage. The results also

show that the prediction of modified D–F model considering a variable  $\alpha$  have a better agreement with the results obtained from virtual experiments, no matter which  $\alpha^2$  curve is adopted. This suggests, on the other hand, that Eq. (17) can replace the complete fitting method in determining the ellipticity. The following analysis with the modified –F model will all use the variable ellipticity determined by uniaxial and hydrostatic compressions (the two-point fitting method).

#### 4.3. Verification of virtual experiments

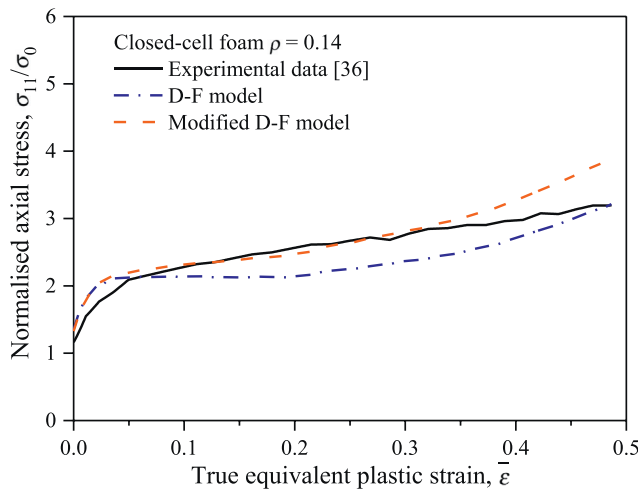
The three most important factors in plastic constitutive relation are the yield condition, hardening law and flow rule. It is no need to consider the flow rule here because the principal stress and principal strain of three directions can all be obtained from the cell-based finite element method. The modified D–F model using a variable  $\alpha$  described in Section 4.2 is adopted here. The hardening law is characterized by the quasi-static stress–strain relation.

The quasi-static stress–strain relations under uniaxial compression were obtained by the virtual experiment, as described in Section 3.2. All data in this paper are processed based on the true stress–strain relation. The nominal stress–strain relation can be converted to the true stress–strain relation as described below. Under uniaxial compression, the true stress is assumed to be equal to the nominal stress and the axial true plastic strain can be obtained by the relation between nominal strain and true (logarithmic) strain that  $\epsilon = -\ln(1 - \epsilon_n)$ , when neglecting the elastic behaviour and the small lateral expansion. In order to be consistent with the traditional nominal stress–strain relation, the coordinate transformation of the final result is carried out. The coordinate transformation does not change the scale of y-axis, but only converts the true strain to the so-called nominal strain with  $\epsilon_n = 1 - \exp(-\epsilon)$  on the x-axis. Then, the true stress–true equivalent plastic strain relation becomes the true stress–nominal equivalent plastic strain, like Figs. 12 and 13.

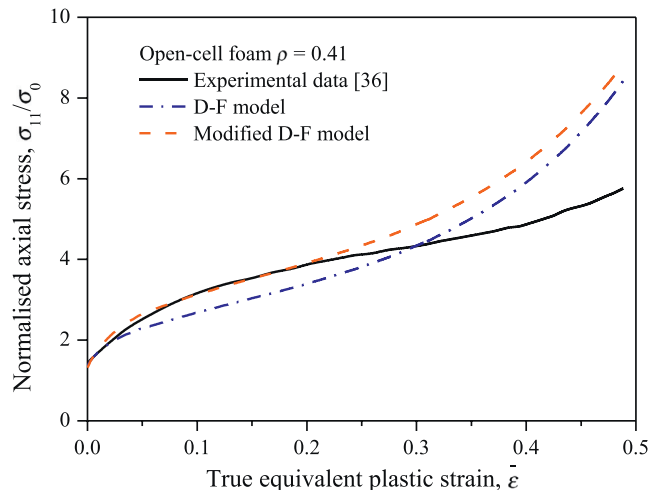
Considering a special proportional compression case, i.e.,  $\sigma_{11}:\sigma_{22}:\sigma_{33} = k:k:1$  ( $k > 1$ ), we have stress triaxiality parameter  $\eta = (2k + 1)/(3k - 3)$  and  $\sigma_e = (k - 1)\sigma_{33} = (k - 1)/k\sigma_{11}$ . The maximum principal stress  $\sigma_1(\bar{\epsilon})$  can be determined by

$$\sigma_1 = \frac{k}{k - 1} \sigma_e = \frac{k\sigma_c}{k - 1} \sqrt{\frac{1 + \alpha^2/9}{1 + \eta^2\alpha^2}} \quad (18)$$

Eq. (18) also applies to the situation when  $\sigma_{11}:\sigma_{22}:\sigma_{33} = k:1:1$ , because it happens that  $\sigma_e = (k - 1)\sigma_{33}$  too. In fact, Eq. (18) is also appli-



(a)



(b)

Fig. 16. Predictions of axial stress of (a) the closed-cell foam and (b) the open-cell foam under proportional compression ( $\eta = 2$ ) from the D–F model with  $\alpha^2 = 0.8$  and the modified D–F model.

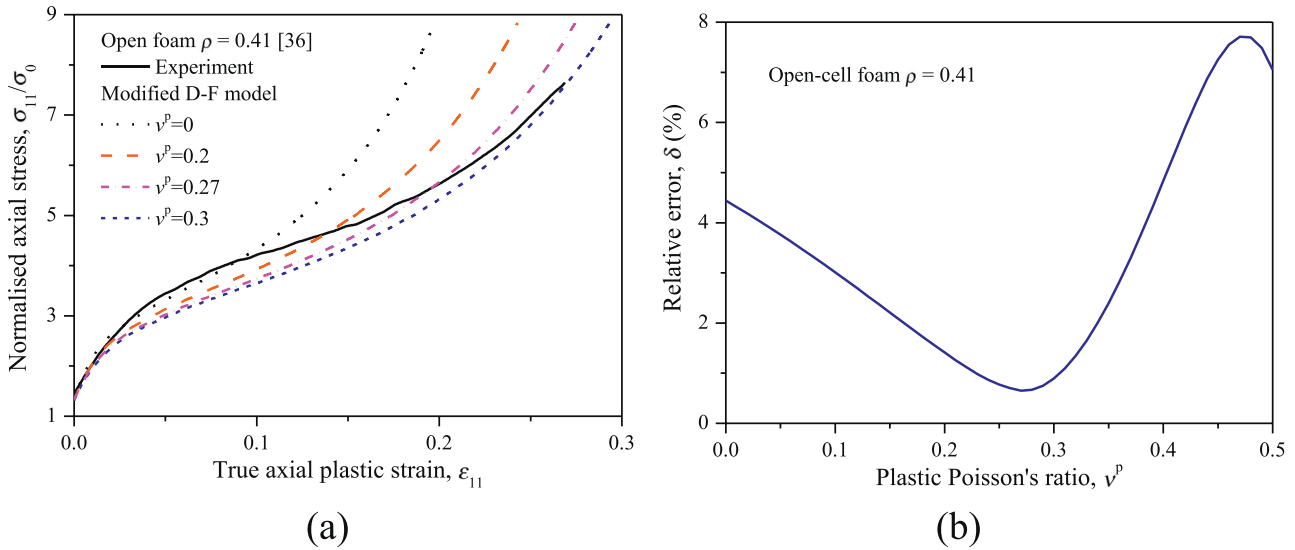


Fig. 17. (a) Predictions of axial stress of the open-cell foam with different plastic Poisson's ratios and (b) the relative square error.

cable for the cases of non-proportional loadings, as long as  $k$  and  $\eta$  are not constants but values vary with strain.

Consider a loading situation when the ratio of the velocity of three principal directions is 5:5:0, which corresponds to a special loading case in experiment that the whole specimen is loaded under a liquid pressure while the axial displacement is constrained to be zero. The ratio of three principal stresses is  $\sigma_1:\sigma_2:\sigma_3 = k:k:1$  ( $k > 1$ ), and the maximum principal stress  $\sigma_1$  can be determined by Eq. (18). Three different relative densities are compared here, i.e., 0.05, 0.1 and 0.15. The D–F model uses scattered uniaxial data and constant  $\alpha^2 = 9/8$ . The modified D–F model adopts the R-PH model to replace scattered uniaxial stress–strain relation and uses the variable ellipticity in Eq. (17) to replace the constant  $\alpha^2 = 9/8$ .

The predictions of the maximum principal stress by the two models are shown in Fig. 13. It can be seen that both the D–F model and modified D–F model can describe the initial stage and densification stage well, but the modified D–F model has a better prediction in the strain range of 0.2 to 0.7. This again verifies that  $\alpha$  should not be a fixed value.

#### 4.4. Verification of experiments

Three kinds of experiments, i.e., uniaxial compression, hydrostatic compression and proportional compression, were conducted by Wang et al. [36]. Two kinds of foams were used: one is a closed-cell foam with a relative density of 0.14 and the other is an open-cell foam with a relative density of 0.41. Uniaxial compression tests were performed with a material test system (MTS 810.23, University of Science and Technology of China) lubricated by the MoS<sub>2</sub>. Hydrostatic compression tests and proportional compression tests were conducted using a Shimadzu EHF-UG digital hydraulic pressure servo 3D test machine (China University of Mining and Technology (Beijing)). The specimens were separated from the oil wrapped by Teflon film to avoid the influence of the outside holes.

For a stress–strain curve with no apparent yield point, the yield point is defined at 0.3% axial plastic strain [11], and the uniaxial yield strength  $\sigma_0$  are 2.4 MPa and 6.3 MPa for the closed-cell foam and open-cell foam, respectively. It is confirmed that the selection of initial crushing stress at other axial plastic strain (0.2% or 0.4%) does not substantially modify the predictions. The uniaxial stress–strain relation and the hydrostatic pressure–volumetric strain curve are plotted in Fig. 14. The square of ellipticity,  $\alpha^2$ , calculated from Eq. (16) is plotted in Fig. 15 which is obviously not constant no matter for the closed-cell foam or the open-cell foam. It is found that  $\alpha^2$  of the closed-cell foam decreases in the form of an approximate exponential function, while  $\alpha^2$

of the open-cell foam first decreases with the increase of the equivalent plastic strain and then increases. Although the microstructure of the experimental foams may be not same with the Voronoi structure used in finite element simulations, the variation characteristics of ellipticity are very similar to that of the Voronoi model mentioned above. So, we also take Eq. (14) to fit  $\alpha^2$ . The fitting equations are

$$\alpha^2 = 0.4559e^{-6.937\varepsilon} + 0.09550\varepsilon^2 + 0.4011 \quad (19)$$

and

$$\alpha^2 = 0.3961e^{-53.65\varepsilon} + 0.8710\varepsilon^2 + 0.4851, \quad (20)$$

for the closed-cell and open-cell foam, respectively, as shown in Fig. 15.

The uniaxial compressive stress–strain data presented in Ref. [36] are some deficiencies, which are lack the data of hardening stage. Thus, it is not sufficient to fit the R-PH model and we will compare the results in the true stress–strain coordinates using the scattered data in the uniaxial compression tests.

The axial stress  $\sigma_{11}$ , i.e., the maximum principal stress, under proportional compression can be deduced from the known uniaxial stress–strain relation, the ellipticity and the stress triaxiality with Eq. (18). The stress triaxiality is  $\eta = 2$  in the proportional compression test. The results are depicted in Fig. 16.

Comparisons between the experimental results in Ref. [36] and the predictions with the D–F model using  $\alpha^2 = 0.8$  and the modified D–F model show that using the modified D–F model with a variable ellipticity  $\alpha$  results in a better agreement, as shown in Fig. 16. It is also noted that the predictions of the modified D–F model deviate from the experimental data when the strain becomes larger than about 0.3, especially for the open-cell foam with a relative density of 0.41. This may be due to the effect of the plastic Poisson's ratio, which becomes significant when the foam has a high relative density.

#### 4.5. Further correction with the plastic Poisson's ratio

As shown in Appendix A, the plastic strain components can be derived from the plastic flow potential which is related to the plastic Poisson's ratio. However, the previous research is based on the assumption that the plastic Poisson's ratio is zero. This assumption may be unacceptable when the relative density of metal foams is high.

The variation of normalised maximum axial stress with axial plastic strain ( $\sigma_{11}/\sigma_0 - \varepsilon_{11}$ ) obtained experimentally in Ref. [36] is compared with predictions of the modified D–F model using different values of plastic Poisson's ratios, as shown in Fig. 17(a). The relative square error

$\delta$ , defined as  $\delta = \sum_1^n ((\sigma_{11}(i) - \sigma_1(i))/\sigma_1(i))^2/n$ , is used to evaluate the influence of plastic Poisson's ratio, where the number of scattered points is  $n = 1000$  and  $\sigma_1$  is the experimental value. It is obvious that the plastic Poisson's ratio has a great influence on the prediction error of the open-cell foam, as illustrated in Fig. 17(b). It can be seen that the prediction error will be smaller than that when the plastic Poisson's ratio is taken as zero, provided the measured plastic Poisson's ratio is between 0 and 0.4 which is almost sure for metal foams. The results also show that the prediction error is the smallest when the plastic Poisson's ratio is about 0.27. Although the plastic Poisson's ratio was not given in Ref. [36] and there are lack of other experimental data for open-cell aluminium foams with a high relative density in the literature, a variable plastic Poisson's ratio is recommended as  $\nu^p = 0.278 - 0.409e^p$  in Ref. [37]. Hence, when considering the influence of the plastic Poisson's ratio, a much better prediction can be obtained. It also indicates that it is necessary to measure the plastic Poisson's ratio in experiments.

## 5. Conclusions

The self-similar isotropic hardening model developed by Deshpande and Fleck [11] has been widely used to describe the constitutive behaviour of metal foams because it is very simple with only two parameters (the ellipticity  $\alpha$  and the uniaxial yield stress  $Y$ ). Cell-based finite element models based on 3D Voronoi technique were used to verify this model in this study.

Seven different loading scenarios, including uniaxial, biaxial and triaxial compressions, are carried out numerically with finite element code ABAQUS/Explicit. The ellipticity is obtained by fitting the results of numerical simulations with the ellipse standard equation. It is found that the ellipticity varies with the equivalent plastic strain. The data of uniaxial and hydrostatic compression tests were used to determine approximately the ellipticity  $\alpha$ . A fitting relation Eq. (14) between the ellipticity and the equivalent plastic strain is suggested. The ellipticity  $\alpha$  is found to be independent of the relative density of cellular material.

The uniaxial stress-strain relation is fitted well with using the R-PH model. A modification to the Deshpande-Fleck foam model with a variable value of ellipticity is suggested. The modified Deshpande-Fleck foam model provides a satisfactory prediction of the post-yield behaviour of the cell-based finite element model of foam with using the variable ellipticity and the R-PH model.

The ellipticity  $\alpha$  determined experimentally by uniaxial compression tests and hydrostatic compression tests is not constant. Good agreement is also observed between the experimentally measured stress-strain responses and the predictions of the modified Deshpande-Fleck foam model using a non-associated flow rule. The prediction becomes better when considering the effect of the plastic Poisson's ratio. It is important to measure the plastic Poisson's ratio to determine the plastic flow potential accurately. Further study is required to measure the plastic Poisson's ratio effectively, or calculate the plastic Poisson's ratio by some characteristic experiments.

## Acknowledgements

This work is supported by the National Natural Science Foundation of China (Projects Nos. 11772330 and 11372308) and the Fundamental Research Funds for the Central Universities (Grant No. WK2480000003).

## Appendix A. A plastic flow rule and the equivalent plastic strain

Inspired by the modified von Mises yield function of Drucker and Prager, the plastic flow potential has been proposed [11, 23, 38]

$$\Phi = \sqrt{\sigma_e^2 + \beta^2 \sigma_m^2}, \quad (\text{A.1})$$

where  $\beta$  represents the shape of the plastic flow potential in the von Mises effective stress vs. mean stress ( $\sigma_e$ - $\sigma_m$ ) plane.

The plastic strains are assumed to be normal to the flow potential  $\Phi$ , written as

$$d\epsilon_{ij} = d\lambda \frac{\partial \Phi}{\partial \sigma_{ij}}, \quad (\text{A.2})$$

where  $d\lambda$  is the non-negative plastic flow multiplier. In a typical proportional loading case, the ratio of three principal stresses is  $\sigma_{11}:\sigma_{22}:\sigma_{33} = k:1:1$  ( $k > 1$ , marked as case I), then the ratio of radial and axial strain rates is given by

$$\frac{d\epsilon_{22}}{d\epsilon_{11}} = \frac{\partial \Phi / \partial \sigma_{22}}{\partial \Phi / \partial \sigma_{11}} = \frac{(1-k) + 2\beta^2(k+2)/9}{2(k-1) + 2\beta^2(k+2)/9}. \quad (\text{A.3})$$

Under uniaxial loading, i.e.,  $k \rightarrow \infty$ , Eq. (A.3) is simplified to

$$\frac{d\epsilon_{22}}{d\epsilon_{11}} = -\frac{1-2\beta^2/9}{2(1+\beta^2/9)}. \quad (\text{A.4})$$

For large deformation, the plastic Poisson's ratio  $\nu^p$  is defined as the negative ratio of the transverse logarithmic strain rate to the axial logarithmic strain rate [11], written as

$$\nu^p = -\frac{\dot{\epsilon}_{22}}{\dot{\epsilon}_{11}} = -\frac{d\epsilon_{22}}{d\epsilon_{11}}. \quad (\text{A.5})$$

Combining Eq. (A.4) with Eq. (A.5) leads to

$$\beta^2 = \frac{9(1-2\nu^p)}{2(1+\nu^p)}. \quad (\text{A.6})$$

The plastic flow rule is non-associated if only the value of  $\beta$  is not the same as the ellipticity  $\alpha$  of yield function. In general, the plastic flow is not associated to the yield function, thus independent calculations of the ellipticity of yield function and the plastic Poisson's ratio are allowed [13, 14, 23]. For many low-density foams, the plastic Poisson's ratio is close to zero, which corresponds to  $\beta \approx 2.12$  as mentioned above.

The  $\sigma_{11}$ - $\bar{\epsilon}$  relation can be converted to the  $\sigma_{11}$ - $\epsilon_{11}$  relation, which is more convenient in comparison with the experimental results. On the basis of the definition of equivalent plastic work, the work conjugate strain rate, i.e., the equivalent plastic strain rate, can be explicitly expressed as [11]

$$\dot{\epsilon} = \sqrt{\left(1 + \frac{\alpha^2}{9}\right) \left(\dot{\epsilon}_e^2 + \frac{\dot{\epsilon}_v^2}{\alpha^2}\right)}, \quad (\text{A.7})$$

where  $\dot{\epsilon}_e = \sqrt{(2/3)\dot{\epsilon}_{ij}\dot{\epsilon}_{ij}}$  is the von Mises effective strain rate and  $\dot{\epsilon}_v = \dot{\epsilon}_{kk}$  the volumetric plastic strain rate. For case I, by combining Eq. (A.3) with  $\eta = \sigma_m / \sigma_e$ , Eq. (A.7) can be re-written as

$$\dot{\epsilon}_{11} = \frac{\alpha(\bar{\epsilon})(1 + \beta^2\eta/3)}{\sqrt{(1 + \alpha^2(\bar{\epsilon})/9)(\alpha^2(\bar{\epsilon}) + \beta^4\eta^2)}} \dot{\epsilon}. \quad (\text{A.8})$$

Integrating Eq. (A.8) with respect to time and considering  $\epsilon_{11} = 0$  and  $\bar{\epsilon} = 0$  at time  $t = 0$ , we can obtain the relation between  $\epsilon_{11}$  and  $\bar{\epsilon}$ . Then,  $\sigma_{11}$ - $\epsilon_{11}$  and  $\sigma_{11}$ - $\bar{\epsilon}$  can be converted to each other.

## References

- [1] Gibson LJ, Ashby MF, Zhang J, Triantafillou TC. Failure surfaces for cellular materials under multiaxial loads—I. modelling. *Int J Mech Sci* 1989;31(9):635–63.
- [2] Gibson LJ, Ashby MF. Cellular solids: structure and properties. 2nd. Cambridge: Cambridge University Press; 1997.
- [3] Rusch KC. Load-compression behavior of flexible foams. *J Appl Polym Sci* 1969;13(11):2297–311.
- [4] Rusch KC. Energy-absorbing characteristics of foamed polymers. *J Appl Polym Sci* 1970;14(6):1433–47.
- [5] Hanssen AG, Hopperstad OS, Langseth M, Ilstad H. Validation of constitutive models applicable to aluminium foams. *Int J Mech Sci* 2002;44(2):359–406.
- [6] Liu QL, Subhash G. A phenomenological constitutive model for foams under large deformations. *Polym Eng Sci* 2004;44(3):463–73.
- [7] Avallé M, Belingardi G, Ibba A. Mechanical models of cellular solids: parameters identification from experimental tests. *Int J Impact Eng* 2007;34(1):3–27.
- [8] Schraad MW, Harlow FH. A stochastic constitutive model for disordered cellular materials: finite-strain uniaxial compression. *Int J Solids Struct* 2006;43(11–12):3542–68.

- [9] Hu LL, Huang XQ, Tang LQ. Constitutive relation of open-celled metal foams based on the mesoscopic behavior of random cells. *Key Eng Mater* 2007;340:403–8.
- [10] Miller RE. A continuum plasticity model for the constitutive and indentation behaviour of foamed metals. *Int J Mech Sci* 2000;42(4):729–54.
- [11] Deshpande VS, Fleck NA. Isotropic constitutive models for metallic foams. *J Mech Phys Solids* 2000;48(6–7):1253–83.
- [12] Chen CQ, Lu TJ. A phenomenological framework of constitutive modelling for incompressible and compressible elasto-plastic solids. *Int J Solids Struct* 2000;37(52):7769–86.
- [13] Zhang J, Lin Z, Wong A, Kikuchi N, Li VC, Yee AF, Nusholtz GS. Constitutive modelling and material characterisation of polymeric foams. *J Eng Mater Technol ASME* 1997;119(3):284–91.
- [14] Zhang J, Kikuchi N, Li VC, Yee AF, Nusholtz GS. Constitutive modeling of polymeric foam material subjected to dynamic crash loading. *Int J Impact Eng* 1998;21(5):369–86.
- [15] Zhang XY, Tang LQ, Liu ZJ, Jiang ZY, Liu YP, Wu YD. Yield properties of closed-cell aluminum foam under triaxial loadings by a 3D Voronoi model. *Mech Mater* 2017;104:73–84.
- [16] Ruan D, Lu GX, Ong LS, Wang B. Triaxial compression of aluminium foams. *Compos Sci Technol* 2007;67(6):1218–34.
- [17] Gioux G, McCormack TM, Gibson LJ. Failure of aluminium foams under multiaxial loads. *Int J Mech Sci* 2000;42(6):1097–117.
- [18] Sridhar I, Fleck NA. The multiaxial yield behaviour of an aluminium alloy foam. *J Mater Sci* 2005;40(15):4005–8.
- [19] Deshpande VS, Fleck NA. Multi-axial yield behaviour of polymer foams. *Acta Mater* 2001;49(10):1859–66.
- [20] Zhou ZW, Wang ZH, Zhao LM, Shu XF. Uniaxial and biaxial failure behaviors of aluminum alloy foams. *Compos Part B Eng* 2014;61:340–9.
- [21] Wu YD, Qiao D, Tang LQ, Liu ZJ, Liu YP, Jiang ZY, Zhou LC. Global topology of yield surfaces of metallic foams in principal-stress space and principal-strain space studied by experiments and numerical simulations. *Int J Mech Sci* 2017;134:562–75.
- [22] Luo G, Xue P, Sun SG. Investigations on the yield behavior of metal foam under multiaxial loadings by an imaged-based mesoscopic model. *Int J Mech Sci* 2018;142:153–62.
- [23] Abaqus analysis user's manual. Version 6.11, Dassault Systems Simulia Corporation, USA, 2011.
- [24] LS-DYNA keyword user's manual. Version 971, Livermore Software Technology Corporation, USA, 2010.
- [25] Reyes A, Hopperstad O.S., Berstad T., Langseth M. Implementation of a Material Model for Aluminium Foam in LS-DYNA. Report R-01-02, Restricted, Department of Structural Engineering, Norwegian University of Science and Technology, 2002.
- [26] Fang H, Bi J, Zhang C, Gutowski M, Palta E, Wang Q. A constitutive model of aluminum foam for crash simulations. *Int J Non-Linear Mech* 2017;90:124–36.
- [27] Alkhader M, Vural M. An energy-based anisotropic yield criterion for cellular solids and validation by biaxial FE simulations. *J Mech Phys Solids* 2009;57(5):871–90.
- [28] Ayyagari RS, Vural M. Multiaxial yield surface of transversely isotropic foams: part I—modeling. *J Mech Phys Solids* 2015;74:49–67.
- [29] Shafiq M, Ayyagari RS, Ehaab M, Vural M. Multiaxial yield surface of transversely isotropic foams: part II—experimental. *J Mech Phys Solids* 2015;76:224–36.
- [30] Zheng ZJ, Wang CF, Yu JL, Reid SR, Harrigan JJ. Dynamic stress-strain states for metal foams using a 3D cellular model. *J Mech Phys Solids* 2014;72:93–114.
- [31] Wang CF, Zheng ZJ, Yu JL. Micro-inertia effect and dynamic plastic Poisson's ratio of metallic foams under compression. *Explos Shock Waves* 2014;34(5):601–7 (in Chinese).
- [32] Combaz E, Bacciarini C, Charvet R, Dufour W, Mortensen A. Multiaxial yield behaviour of Al replicated foam. *J Mech Phys Solids* 2011;59(9):1777–93.
- [33] Shaw MC, Sata T. The plastic behavior of cellular materials. *Int J Mech Sci* 1966;8(7):469–78.
- [34] Yang J, Wang SL, Ding YY, Zheng ZJ, Yu JL. Crashworthiness of graded cellular materials: a design strategy based on a nonlinear plastic shock model. *Mater Sci Eng A* 2017;680:411–20.
- [35] Yu JL, Wang EH, Li JR. An experimental study on the quasi-static and dynamic behavior of aluminum foams under multi-axial compression. In: Fan JH, Chen HB, editors. *Advances in Heterogeneous Material Mechanics*. Lancaster: DEStech Publications; 2008. p. 879–82.
- [36] Wang EH, Yu JL, Wang F, Sun L. A theoretical and experimental study on the quasi-static constitutive model of aluminum foams. *Acta Mech Sin* 2004;36(6):673–9 (in Chinese).
- [37] Su YS, Gong XL. An analytical stress-strain model for open-cell metal foam. *J Porous Media* 2012;15(12):1137–45.
- [38] Drucker DC, Prager W. Soil mechanics and plastic analysis or limit design. *Q Appl Math* 1952;10:157–65.